Rare Metal Materials and Engineering
Volume 55, Issue 1, January 2026
Available online at www.rmme.ac.cn

Science Press

Cite this article as: Li Linzi, Guan Xianjun, Hou Jieshan, et al. Influence of Hf Alloying on Precipitation Behavior of γ′ Phase and Tensile Properties of Ni-Cr-Mo Alloy[J]. Rare Metal Materials and Engineering, 2026, 55(01): 59-66. DOI: https://doi.org/10.12442/j.issn.1002-185X.20240815.

ARTICLE

Influence of Hf Alloying on Precipitation Behavior of γ′ Phase and Tensile Properties of Ni-Cr-Mo Alloy

Li Linzi[1,2], Guan Xianjun[1,3], Hou Jieshan[1,3], Zhou Lanzhang[1,3]

[1] Shi-changxu Innovation Center for Advanced Materials, Institute of Metal Research, Chinese Academy of Sciences, Shenyang 110016, China; [2] School of Materials Science and Engineering, University of Science and Technology of China, Shenyang 110016, China; [3] CAS Key Laboratory of Nuclear Materials and Safety Assessment, Institute of Metal Research, Chinese Academy of Sciences, Shenyang 110016, China

Abstract: The influence of Hf on the precipitation behavior of γ′ phase and the subsequent tensile properties of a Ni-Cr-Mo alloy after long-term thermal exposure was investigated. The results reveal that the addition of Hf increases the average diameter of γ′ phases after thermal exposure at 700 ℃ for 5000 h, which enhances the critical resolved shear stress required for dislocations to shear the γ′ phases in the Ni-Cr-Mo alloy. Simultaneously, element Hf incorporated into the γ′ phases increases the lattice mismatch between the γ′ and γ phase, thereby strengthening the coherency strengthening effect. These two factors collectively contribute to the enhanced strength of the alloy. Thus, Hf alloying effectively improves the yield strength of the Ni-Cr-Mo alloy after thermal exposure at 700 ℃.

Key words: Ni-Cr-Mo alloy; Hf alloying; γ′ strengthening; long-term thermal exposure; dislocations shearing

1 Introduction

To address the growing challenges of environmental pollution and energy shortage, the development of advanced ultra-supercritical (A-USC) high-power plants holds great significance. These plants can effectively reduce the cost of burning coal and greenhouse gas emission[1–2]. According to the basic principle of the Carnot cycle, increasing the temperature and pressure of the main steam is critical for improving the thermal efficiency of A-USC power plants[3–4]. However, the elevated operating parameters put forward higher requirements on the high temperature performance of structural materials used in A-USC power plants, e.g., excellent tensile properties and oxidation resistance. Nowadays, the maximum applicable temperature of ferritic steels in turbine units is limited to 650 ℃. For A-USC generating units with higher parameters, γ′-reinforced Ni-based superalloys are more suitable. Normally, the A-USC high-power plants typically serve for up to 30 years. In this case, besides excellent initial performance, exceptional microstructure and performance stability of candidate materials is of great significance[5–6]. Ni-based superalloys have become the ideal materials for key components in ultra-supercritical (USC) boiler systems at 700 ℃, due to their exceptional high-temperature oxidation/corrosion resistance, superior elevated-temperature strength, creep resistance, and stress-rupture properties[7–8]. In γ′-strengthened Ni-based superalloys, the overall properties are largely determined by their chemical composition.

In the present work, a Ni-Cr-Mo alloy was selected as the target material, which contains a high content of solution-strengthening elements (e.g., Cr, Mo, and Nb) and a small number of precipitation-strengthening elements (e.g., Al and Ti). The original design strategy of this alloy was to achieve favorable microstructural stability and excellent high-temperature corrosion resistance. Firstly, a higher proportion of Cr is used in the alloy. On the one hand, element Cr can enhance the oxidation and hot corrosion resistance[9–10]. On the other hand, as a solid solution element, Cr dissolves in the γ matrix, producing a solid-solution strengthening effect. Simultaneously, Cr can increase the cubicity of γ′ and the

Received date: January 16, 2025
Foundation item: National Key Research and Development Program of China (2021YFB3704103); National Natural Science Foundation of China (51571191)
Corresponding author: Hou Jieshan, Ph. D., Associate Professor, Shi-changxu Innovation Center for Advanced Materials, Institute of Metal Research, Chinese Academy of Sciences, Shenyang 110016, P. R. China, E-mail: jshou@imr.ac.cn; Zhou Lanzhang, Ph. D., Professor, Shi-changxu Innovation Center for Advanced Materials, Institute of Metal Research, Chinese Academy of Sciences, Shenyang 110016, P. R. China, E-mail: lzz@imr.ac.cn

lattice mismatch degree between γ' and γ[11–12]. Element Mo, when entering the matrix, enhances the lattice distortion of the γ phase, thus producing significant solid-solution strengthening effect[13]. Certainly, Mo alloying increases the anti-phase boundary (APB) energy of γ', which further enhances the precipitation-strengthening effect[14]. Meanwhile, Al and Ti in the alloy can optimize mechanical properties by forming γ' precipitates. In this case, the mechanical properties are closely related to the γ' characteristics[15–17].

For element Hf, it is believed that an addition of Hf can improve mechanical properties through grain boundary strengthening mechanisms, such as reducing the tendency for grain boundary tearing, preventing grain boundary embrittlement caused by sulphur, and enhancing resistance to hold-time-crack growth[18–19]. Wu et al[20] studied the influence of lattice mismatch on mechanical behavior and the ductility effect of Hf in the Ni-Ni_3Al system by first-principles calculation. Their findings indicated that Hf is preferentially segregated in the γ' phase instead of the γ matrix and occupies the Al sites rather than Ni sites in the γ' phase. Zhang et al[21–22] studied the partitioning of Hf among phases by atom probe tomograph and its effects on γ/γ' misfit by X-ray diffraction (XRD) in FGH97 PM superalloy. Their results revealed two key observations: first, Hf is primarily distributes in the γ' phase, altering its composition from $(Ni, Co)_3(Al, Ti, Nb)$ to $(Ni, Co)_3(Al, Ti, Nb, Hf)$, which enhances both the content and lattice constant of γ' precipitates; second, adding an appropriate amount of Hf reduces γ/γ' misfit, which is conducive to high-temperature durability enhancement of the alloy. These studies collectively demonstrate that the addition of Hf plays an important role in regulating the γ' phase in general Ni-based superalloys.

Our recent research on a Ni-Cr-Mo alloy[23] has shown that at as-cast state, the alloy contains a large number of secondary phases, including relative coarse γ', *M*C carbide, etc, and the majority of these precipitates redissolve into the matrix after solid solution treatment. Furthermore, γ' reprecipitates to strengthen the alloy during the subsequent thermal exposure process. For γ'-strengthened Ni-Cr-Mo alloys, their mechanical properties can be regulated by Hf alloying. Therefore, this study focuses on the effects of Hf on the precipitation behavior of γ' and the resulting tensile properties. The findings are expected to offer novel insights and ideas for the composition design of such Ni-based superalloys.

2 Experiment

The Ni-Cr-Mo alloy investigated in the present work has a nominal composition of Ni-22Cr-12(Mo+Nb)-2(Al+Ti)-0.03C (wt%), which was named as Hf-free alloy. The Hf-doped alloy was obtained by adding 0.5wt% Hf to the Hf-free alloy. Both alloys were melted in a vacuum induction furnace, and cast into rods with 16 mm in diameter and 80 mm in length.

The as-cast alloys were subjected to solution treatment at 1200 ℃ for 1 h, followed by water cooling. This heat treatment can reduce dendritic elemental segregation and dissolve secondary phases to obtain supersaturated solid solution[24–27]. To investigate the influence of Hf alloying on the evolution of γ' phase, the alloys were thermally exposed at 700 ℃ for 1000, 3000, and 5000 h.

Standard tensile samples with a diameter of 14 mm and a gauge length of 25 mm were adopted in the present work. Uniaxial tensile tests were performed on an AG-250kN universal testing machine at 700 ℃. The samples for scanning electron microscope (SEM) observation were ground, mechanically polished, and then electrochemically etched by an etchant solution consisting of 150 mL H_3PO_4+10 mL H_2SO_4+15 g CrO_3, with a applied current of 1 A for 5–10 s. The γ' morphologies and elemental segregation were characterized using an Inspect F50 field emission SEM equipped with energy dispersive X-ray spectroscope (EDS). The samples for transmission electron microscope (TEM) observation with EDS analysis were ground to 50 μm in thickness and twin-jet polished in a solution of 10vol% perchloric acid at a voltage of 30 V and a temperature of –25 ℃. A JEOL 2100FX TEM operating at 200 kV was used to investigate the interaction between dislocations and γ' phases, while a TECNAI G2 F30 TEM was employed to analyze γ' composition through high-angle annular dark-field (HAADF) imaging. XRD measurements were conducted using a D/Max-2500PC diffractometer at an accelerating voltage of 45 kV and a scanning speed of 20°/min. XRD data were analyzed by JADE 6.0 software.

The effects of Hf on γ' evolution are reflected in Al segregation which can be expressed by the segregation ratio, $R = C_d/C_i$, where C_d and C_i are the concentrations of Al in the dendrite cores and interdendrite areas, respectively. To determine C_d and C_i, EDS analyses of element Al on the two alloys at different states were conducted. Elemental activities were calculated using the Thermal-Calc software with the Ni-V5 Databases.

3 Results and Discussion

3.1 Tensile properties of Hf-free and Hf-doped alloys at 700 ℃

Fig.1 exhibits the yield strength (YS) and area reduction (φ) of Hf-free and Hf-doped alloys at 700 ℃ as a function of thermal exposure time. Obviously, the YS of the two alloys

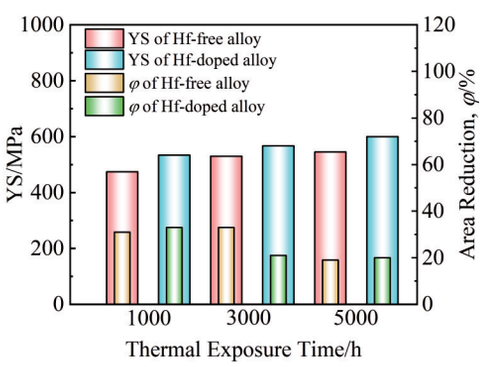

Fig.1 Effect of thermal exposure time on YS and area reduction for Hf-free and Hf-doped alloys at 700 ℃

increases with prolonging the exposure time. Specifically, the YS values of Hf-free and Hf-doped alloys exposed at 700 ℃ for 1000 h are 474 and 534 MPa, respectively. As the thermal exposure time is extended to 5000 h, the YS of both alloys increases by 12%–15%. It is worth noting that the Hf-doped alloy exhibits higher YS than the Hf-free alloy across all exposure durations. The YS of the Hf-doped alloy increase slightly by about 12%, when the thermal exposure time is prolonged from 1000 h to 5000 h. In contrast to the YS trends, the area reductions of both Hf-free and Hf-doped alloys decrease after long-term thermal exposure. Specifically, the area reduction of the Hf-free alloy after thermal exposure for 1000 h is 31%. Upon prolonging the thermal exposure time to 5000 h, the area reduction of the Hf-free alloy decreases by 38%. Comparatively, after 1000 h of thermal exposure, the area reduction of Hf-doped alloy shows a 6.5% improvement, compared with that of the Hf-free alloy. However, it deteriorates significantly when exposure time reaches 3000 h, which is earlier than the deterioration onset of the Hf-free alloy. As the thermal exposure time is further prolonged, the area reduction of Hf-doped alloy is relatively stable. The influences of Hf on these properties are closely related to the variations of γ' in different alloys during long-term thermal exposure.

3.2 Influences of Hf alloying on γ' evolution during long-term thermal exposure at 700 ℃

Fig. 2 displays the morphologies of Hf-free and Hf-doped alloys after long-term thermal exposure at 700 ℃ for 1000, 3000, and 5000 h. In all alloys, the γ' phases exhibit spherical morphologies, though minor differences in size are observed between the two alloys. First, with prolonging the thermal exposure time, the γ' size in the two alloys increases obviously. Second, variations in γ' size between the Hf-free and Hf-doped alloys are evident across different exposure durations. Specifically, after 1000 h of thermal exposure, the γ' phases are relatively small: the Hf-free alloy has γ' phases with an average diameter of 31 nm, while the Hf-doped alloy has γ' phases with a slightly larger average diameter of 37 nm. Certainly, the volume fraction of γ' in Hf-doped alloy is also higher than that in the Hf-free alloy. This phenomenon is in agreement with the findings in Ref.[28–29], which report that Hf alloying promotes the γ' precipitation. When the thermal exposure time is prolonged to 3000 h, the γ' diameter increases to 44 nm in the Hf-free alloy, whereas the average γ' size of the Hf-doped alloy reaches 52 nm. After thermal exposure for 5000 h, the γ' size increases to 62 nm in the Hf-free alloy and 67 nm in the Hf-doped alloy. The increased γ' size results in the decrease in channel width of γ, limiting the space for dislocation motion, and impairing deformability. Thus, the plasticity significantly decreases after long-term thermal exposure. Furthermore, in the present work, the standard deviation (std) of γ' sizes was calculated as an indicator of γ' dispersion uniformity (Fig. 3). Obviously, the larger the standard deviation, the more inferior the γ' distribution uniformity. With prolonging the thermal exposure time, the standard deviation of γ' sizes increases in both the Hf-free and Hf-doped alloys, which should be attributed to continuous precipitation of γ' phases.

In Ni-Cr-Mo superalloys, γ' coarsening is often controlled by elemental diffusion, which obeys Lifshitz-Slyozov-Wagner (LSW) theory[30–31]. This theory assumes that the average diameter of γ' and the thermal exposure time follow a specific relationship, as expressed in Eq.(1).

$$d^3 - d_0^3 = kt \quad (1)$$

where d is the average diameter of γ' after thermal exposure for t h, d_0 is the initial average diameter of γ' without thermal exposure, t is the thermal exposure time, and k is the

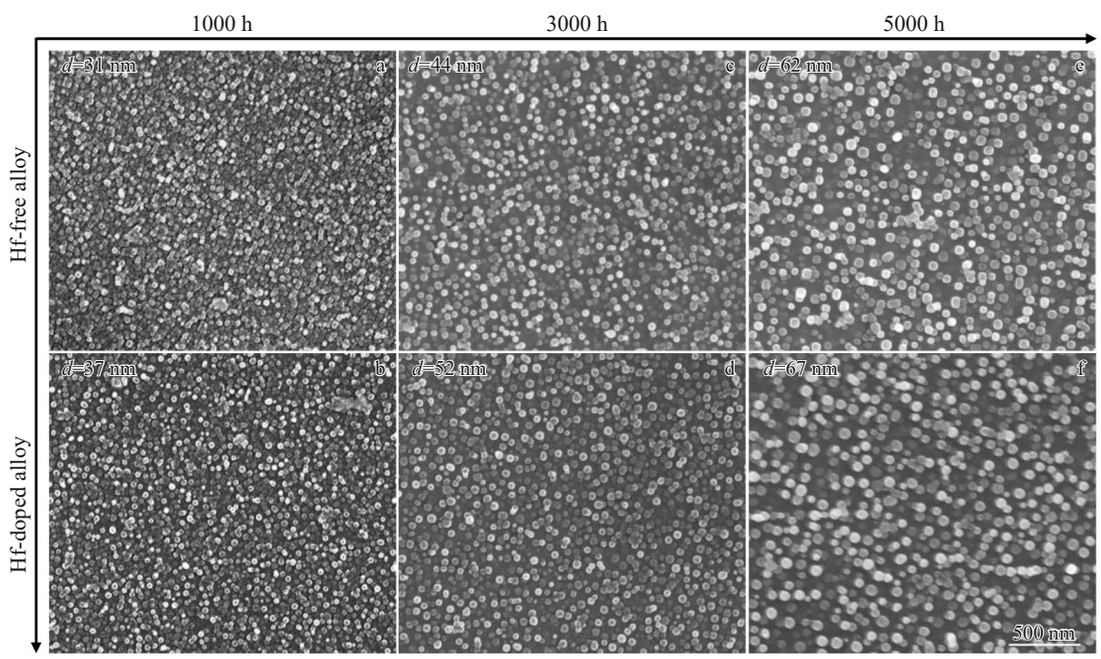

Fig.2 Morphology evolution of γ' phases in Hf-free alloys (a, c, e) and Hf-doped alloys (b, d, f) after thermal exposure at 700 ℃ for different durations: (a–b) 1000 h, (c–d) 3000 h, and (e–f) 5000 h

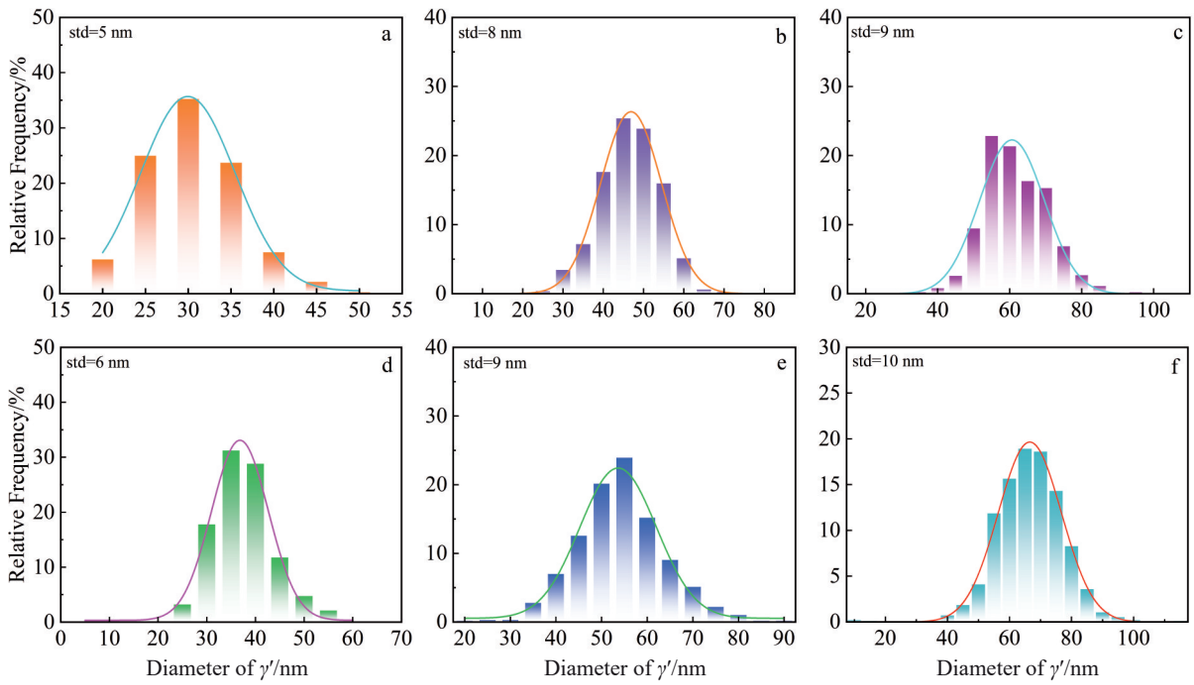

Fig.3 Size distributions of γ' phases in Hf-free alloys (a–c) and Hf-doped alloys (d–f) after thermal exposure at 700 °C for different durations: (a, d) 1000 h, (b, e) 3000 h, and (c, f) 5000 h

coarsening coefficient.

In this study, the k values for the Hf-free and Hf-doped alloys are determined to be 46 and 52 nm^3/h, respectively. It is well known that the k value is controlled by the diffusion rate of γ'-forming elements[32]. Previous works have indicated that the diffusion activation energy of Hf (Q=251 $kJ\cdot mol^{-1}$) is lower than that of Al (Q=260 $kJ\cdot mol^{-1}$) in Ni[33]. Moreover, Hf can be incorporated into the γ' phase and enhance the coarsening rate of γ'[28–29]. Hence, the k value of the Hf-doped alloy is larger than that of the Hf-free alloy.

In addition to the size of γ', the lattice mismatch between γ and γ' precipitates is another important factor affecting the mechanical properties.

3.3 Effect of Hf alloying on lattice mismatch between γ and γ'

In both alloys, the γ' precipitates maintain a coherent relationship with the γ matrix, causing the diffraction peaks of γ' and γ to overlap in XRD patterns. Thus, the peaks must be deconvolved using the PersonVII function in PeakFit software. For the Hf-free and Hf-doped alloys after thermal exposure for 5000 h, the (111) plane with the highest diffraction intensity is selected to calculate the lattice parameters of γ and γ'. This calculation employs the Bragg equation[5,7], $2d\sin\theta = n\lambda\,(n = 1)$, and the interplanar spacing formula for face-centered cubic crystal, $1/d = \sqrt{h^2 + k^2 + l^2}/a$. a is the lattice constant. The lattice mismatch (δ) between γ and γ' precipitates is calculated using the equation: $\delta = 2(a_{\gamma'} - a_{\gamma})/(a_{\gamma'} + a_{\gamma})$. a_{γ} and $a_{\gamma'}$ mean the lattice constants of γ and γ', respectively. Furthermore, to obtain accurate intensity distributions, a fine XRD scan is performed on the (111) plane, as shown in Fig.4. The lattice constants of γ and γ' and the lattice mismatch (δ) for both the Hf-free and Hf-doped alloys are presented in Table 1. Hf alloying results in larger lattice parameters of γ' and γ, increasing by 0.06% and 0.28%, respectively. As a large-sized atom, most Hf in the alloy enters into the γ' phase, leading to stronger lattice distortion, and thus

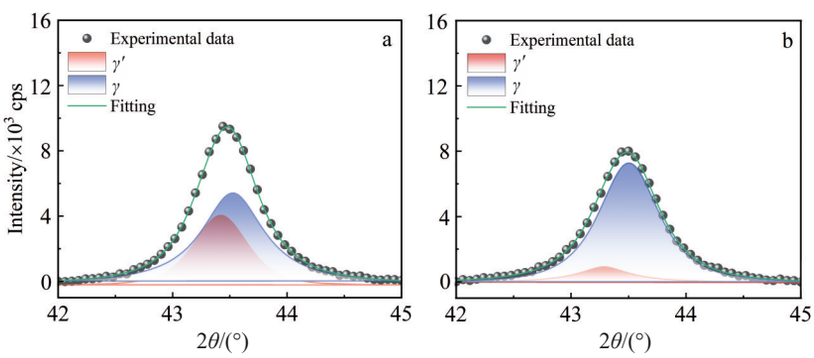

Fig.4 XRD patterns of the (111) plane for the Hf-free (a) and Hf-doped (b) alloys after thermal exposure at 700 °C for 5000 h

Table 1 Lattice constants and δ of Hf-free and Hf-doped alloys after long-term thermal exposure at 700 ℃ for 5000 h

Alloy	a_γ/×10^{-1} nm	$a_{\gamma'}$/×10^{-1} nm	δ/%
Hf-free	3.598	3.607	0.25
Hf-doped	3.600	3.617	0.47

inducing a higher increase magnitude in γ' lattice constant compared to that of γ. Therefore, the δ of the Hf-doped alloy is larger than that of the Hf-free alloy, which can enhance the precipitation-strengthening effect.

3.4 γ' strengthening mechanism of Hf-free and Hf-doped alloys

The enhancement of lattice mismatch caused by Hf alloying can also result in improvement in coherency strengthening, which is expressed by Eq.(2)[34].

$$\tau_c = 6G(d/2b)^{1/2} f^{1/2} \delta_H^{3/2} \quad (2)$$

where τ_c denotes coherency strengthening stress, G is the shear modulus, d is the average diameter of γ', b is the value of Burgers vector, f is the volume fraction of γ', and δ_H is the lattice mismatch between γ and γ' at high temperatures.

It is well known that δ_H is closely related to the thermal expansion coefficient of the γ/γ' phases at high temperatures[35–36]. Combining the thermal expansion coefficients of the γ/γ' phases in both the Hf-free and Hf-doped alloys, the lattice mismatches of both alloys at high temperatures can be expressed as δ_H=0.71δ (for the Hf-free alloy) and δ_H=0.79δ (for the Hf-doped alloy), respectively. On the basis of previous studies and thermodynamic calculations[37–38], the relevant parameters are as follows: G=61.73 GPa, b=0.254 nm, $f_{\text{Hf-free alloy}}$=14.84%, $f_{\text{Hf-doped alloy}}$=15.53%, $\delta_{\text{Hf-free alloy}}$=0.0024, and $\delta_{\text{Hf-doped alloy}}$=0.0047. Substituting these parameter values into Eq.(2) yields the curves of coherency strengthening stress (τ_c) versus γ' diameter, which are plotted in Fig. 5. Obviously, the τ_c derived from coherency strengthening increases after Hf-alloying. Furthermore, with the increase in γ' diameter, the coherency-strengthening effect is enhanced.

In addition to coherency strengthening, both alloys are strengthened through γ'-induced precipitation strengthening during the tensile process. The γ' strengthening mechanism is mainly manifested in two modes: dislocations shearing γ' and

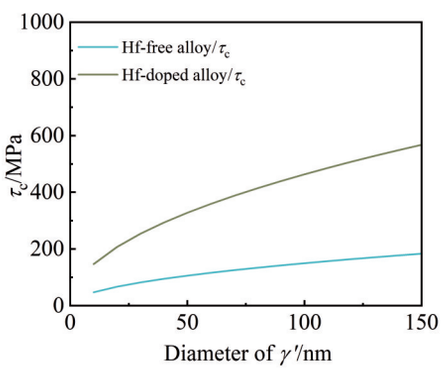

Fig.5 Curves of theoretical τ_c vs γ' diameter for Hf-free and Hf-doped alloys

the dislocations bypassing γ'. To identify the dominant strengthening mechanism in these two alloys, the critical resolved shear stress (CRSS) is calculated. As the diameter of γ' is smaller than the spacing of dislocation pairs, the two dislocations in pairs cannot shear the same γ' phase at the same time. In this case, a weakly coupled dislocation (WCD) interaction occurs between γ' and the dislocation pairs. The CRSS induced by WCD ($\Delta\tau_w$) can be calculated using Eq.(3)[39–41]:

$$\Delta\tau_w = \frac{1}{2}(\gamma_{APB}/b)^{3/2}(2df/Gb)^{1/2}A - \frac{1}{2}(\gamma_{APB}/b)f \quad (3)$$

where γ_{APB} is the antiphase boundary energy, d is the average diameter of γ', G is the shear modulus, f is the volume fraction of γ', and A is the shape factor depending on the morphology of γ'.

With prolonging the thermal exposure time, γ' undergoes coarsening. As the diameter of γ' is larger than the spacing of paired dislocations, the two dislocations in a pair can shear the same γ' phase simultaneously. Strongly coupled dislocation (SCD) interaction happens between γ' and the dislocation pairs. The CRSS induced by SCD ($\Delta\tau_s$) can be expressed by Eq.(4)[39–41]:

$$\Delta\tau_s = \frac{1}{2} \times 1.72(Gb\omega/2d) f^{1/2} [1.28(2d\gamma_{APB}/Gb^2\omega) - 1]^{1/2} \quad (4)$$

where ω is a parameter associated with elastic interaction between paired dislocations.

Besides, the dislocation bypassing γ' follows the Orowan bow-bending mechanism. In this case, the CRSS caused by Orowan bow-bending mechanism ($\Delta\tau_o$) can be calculated by Eq.(5)[42]:

$$\Delta\tau_o = Gb\varphi \ln(L/2b)/2\pi L \quad (5)$$

$$\varphi = 1/\{2[1 + 1/(1+\mu)]\} \quad (6)$$

where μ is the Poisson's ratio; L is the interparticle distance of γ'. L depends on the size and volume fraction of γ', so L is expressed by Eq.(7)[43]:

$$L = d[\sqrt{(8/3\pi f)} - 1] \quad (7)$$

According to previous investigations and thermodynamic calculations[37–38], the following parameters are obtained: γ_{APB}= 0.1 J/m^2, b=0.254 nm, A=0.72 (for spherical γ'), ω=1, G=61.73 GPa, $f_{\text{Hf-free alloy}}$=14.84%, and $f_{\text{Hf-containing alloy}}$=15.53%. Substituting these data into Eq. (3 – 7) yields the relationships between CRSS and γ' diameter for the Hf-free and Hf-doped alloys, which are plotted in Fig. 6a. The ordinate $\Delta\tau$ refers to the resistance that dislocations must overcome to shear the γ' precipitates. Therefore, the critical γ' diameters for the transformation from WCD to SCD interactions are determined to be 66 and 67 nm for the Hf-free and Hf-doped alloys, respectively.

In the present work, the average γ' diameter in both the Hf-free and Hf-doped alloys is smaller than their respective critical diameters. Thus, γ' strengthening mainly derives from WCD. Intuitively, the variations of YS with γ' size in the two alloys are also displayed in Fig.6a. Distinctly, the variations of YS of both alloys closely align with the $\Delta\tau_w$. Correspondingly, the main interaction between dislocations and γ' is also detected by TEM in Hf-doped alloy after thermal exposure for 5000 h (Fig. 6b). Obviously, the left arrow refers to stacking

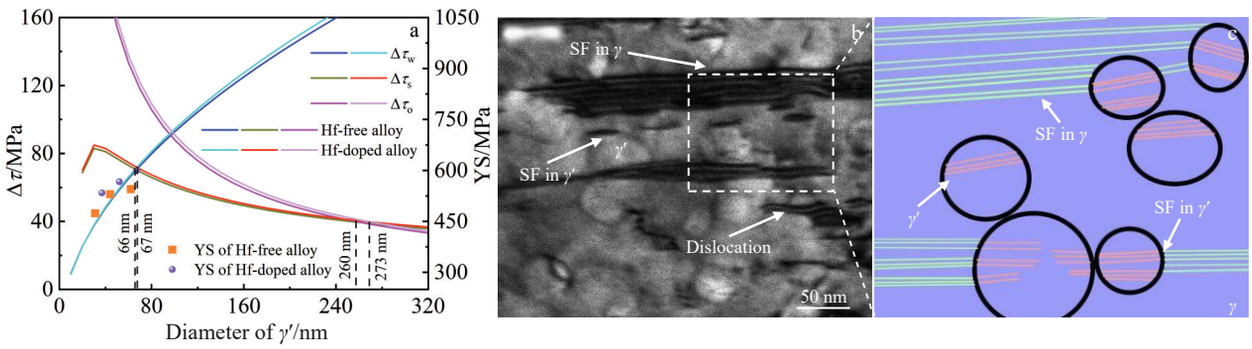

Fig.6 Theoretical CRSS and YS vs γ' diameter for Hf-free and Hf-doped alloys (a); TEM image showing the interaction between dislocations and γ' in Hf-doped alloy thermally exposed at 700 ℃ for 5000 h (b); schematic illustration of dislocation interaction with γ' (c) (salmon lines refer to the stacking faults generated by the dislocations shearing γ, green lines refer to the stacking faults induced by the dislocations shearing γ', and black circles represent γ' precipitates)

faults (SFs) generated by dislocations shearing γ'; the top arrow refers to SFs caused by the dislocations shearing γ. Schematic illustration (Fig. 6c) of the dashed box in Fig. 6b confirms the dislocations shearing γ' in the manner of WCD.

In the WCD-dominated mechanism, the strength from γ'-strengthening is controlled by γ' size, which increases with the increase in γ' diameter. Across all thermal exposure durations, the average γ' diameter in the Hf-doped alloys is larger than that in the Hf-free alloys. Therefore, the YS originated from WCD is higher in the Hf-doped alloys than in the Hf-free alloy. Thus, under the influence of the above two factors, the YS of the alloys is effectively improved.

Actually, the variation in γ' size in the Hf-doped alloys is highly related to the influence of Hf alloying on the Al distribution.

3.5 Effects of Hf alloying on Al segregation

As the most important γ'-forming element, Al exerts a crucial influence on the formation and evolution of γ' precipitates. Previous study[44] illustrated that the content and distribution of Al could significantly affect the precipitation behavior of γ'. Certainly, the precipitation behavior of γ' can also reversely influence the distribution characteristics of Al. Therefore, the effects of Hf alloying on γ' evolution can be explained by analyzing the variation in Al distribution between Hf-free and Hf-doped alloys. EDS data for the two alloys after thermal exposure for 0 (solution treatment), 3000, and 5000 h are plotted in Fig.7. Obviously, Al is segregated in the dendritic cores of the Hf-free alloys, while it is segregated in the interdendritic regions for the Hf-doped alloys. In the solution-treated samples, the segregation ratio of the Hf-free alloys is higher than that of the Hf-doped alloy. With prolonging the thermal exposure duration, the segregation ratios of Al in the two alloys gradually approach 1, which indicates that the degree of Al segregation decreases in both Hf-free and Hf-doped alloys. Specifically, during thermal exposure up to 5000 h, the segregation ratio of Al drops in Hf-free alloy but rises in Hf-doped alloy. For the Hf-free alloy, the size and volume fraction of γ' increase continuously with prolonging the exposure time. Furthermore, this process proceeds more quickly in dendrite cores, where Al content is higher, leading to faster consumption of Al in the γ matrix. Thus, the difference in Al content between dendritic cores and interdendritic regions decreases in the Hf-free alloys. For Hf-doped alloys, Hf participates in forming γ', and some Al atoms in γ' are replaced by Hf. EDS element mapping results of γ' in the Hf-doped alloys are exhibited in Fig. 8. The distinct contrast of Al and Hf in γ' implies their substantial presence (Fig. 8b and 8d), while the dark contrast of Cr suggests its scarcity in γ' (Fig. 8c). In this case, the consumption of Al in the γ matrix is restrained during the formation of γ'. Therefore, the difference in Al content between dendritic cores and interdendrite regions also decreases gradually in the Hf-doped alloy.

From another perspective, the influence of Hf alloying on Al segregation behavior can be attributed to variations in Al activity. Activity is the thermodynamic equilibrium concentration of a component and it is commonly used to characterize the alloying degree of that component. Based on the Miedema model[45], the activities of Al in the alloy at 700 °C were analyzed using Thermal-Calc software with the Ni-V5 database. The results reveal that the Hf alloying reduces the Al activity from 1.890×10^{-10} to 1.877×10^{-10}, rendering it harder to diffuse in the Hf-doped alloy.

The pivotal factor underlying Hf impeding Al consumption in γ' precipitation can be attributable to its notably higher

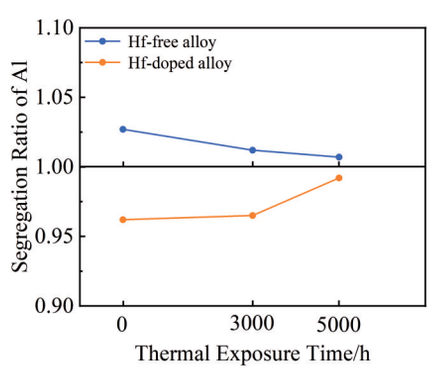

Fig.7 Variations of Al segregation behavior in Hf-free and Hf-doped alloys with thermal exposure time at 700 ℃

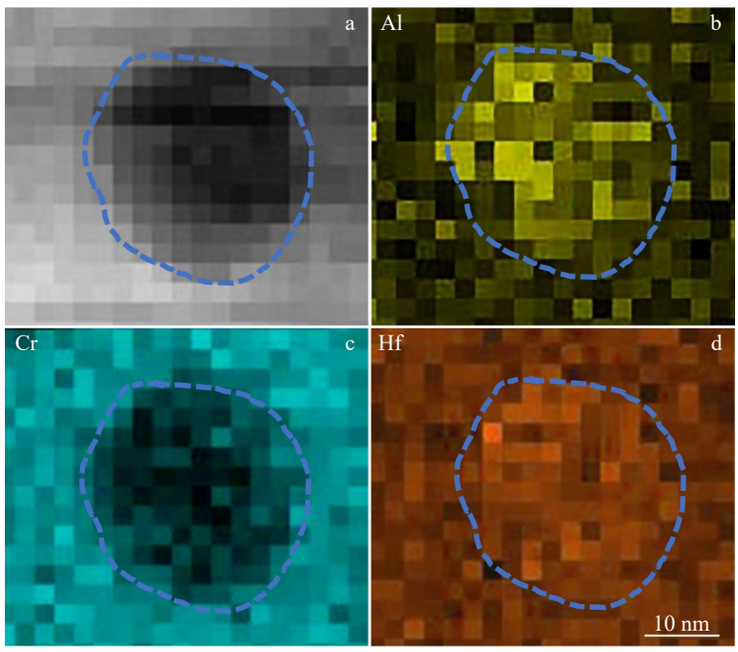

Fig.8 HAADF image of the γ' in Hf-doped alloy after thermal exposure at 700 ℃ for 3000 h (a) and corresponding EDS mappings of elements Al (b), Cr (c), and Hf (d)

diffusion rate in comparison to Al. After solid-solution treatment, most precipitates dissolve into the matrix. During long-term thermal exposure at 700 ℃, elements Al and Hf gradually diffuse. From the thermodynamic perspective, the diffusion activation energy of Hf in Ni (251 kJ·mol^{-1}) is lower than that of Al in Ni (260 kJ·mol^{-1})[33]. Hence, Hf can diffuse more easily than Al, which is more conducive to the formation of γ'. Eventually, compared with that in the Hf-free alloys, the γ' diameter in the Hf-doped alloy increases markedly after long-term thermal exposure at 700 ℃.

In summary, the influence of Hf on the mechanical properties of the Ni-Cr-Mo alloy can be mainly ascribed to the following two aspects. On the one hand, Hf diffuses more rapidly than Al, and exerts a stronger promotion effect on γ' formation. This results in a larger γ' size in the Hf-doped alloy compared to the Hf-free alloys. In γ'-strengthened Ni-Cr-Mo alloys, the strength contributed by γ' strengthening is mainly controlled by γ' size; this strengthening is achieved through WCD mechanism, where dislocations shear γ'. On the other hand, Hf atoms are incorporated into the γ' precipitates, leading to a higher lattice mismatch between γ and γ', which further improves the strengthening effect.

4 Conclusions

1) With prolonging the thermal exposure time, the YS of both Hf-free and Hf-doped Ni-Cr-Mo alloys gradually increases, and the YS of Hf-doped alloys is consistently higher than that of Hf-free alloys.

2) During long-term thermal exposure of the Ni-Cr-Mo alloy, Hf alloying increases the average diameter of γ' precipitates. Furthermore, Hf alloying enhances the lattice mismatch between the γ matrix and γ' precipitates after thermal exposure at 700 ℃ for 5000 h.

3) In γ'-strengthened Ni-Cr-Mo alloys, the strength contributed by γ' strengthening is mainly controlled by γ' precipitates. This strengthening is achieved via WCD mechanism, where dislocations shear the γ' particles.

4) Hf atoms enter the γ' phase, leading to a higher lattice mismatch between γ and γ', and thereby further improving strengthening effect.

5) Based on the analysis of strengthening theory, the improvement in the alloy's strength is primarily attributable to the increase in average diameter of γ' precipitates.

References

1 Viswanathan R, Henry J F, Tanzosh J *et al. Journal of Materials Engineering and Performance*[J], 2005, 14(3): 281

2 Gao S, Hou J S, Yang F *et al. Journal of Alloys and Compounds*[J], 2017, 729: 903

3 Dubiel B, Czyrska-Filemonowicz A. *Materials Chemistry and Physics*[J], 2003, 81(2–3): 427

4 Wu Y S, Zhang M C, Xie X S. *Procedia Engineering*[J], 2015, 130: 617

5 Yang F, Hou J S, Zhou L Z. *Philosophical Magazine Letters*[J], 2020, 101(2): 85

6 Jablonski P D, Hawk J A, Cowen C J *et al. JOM*[J], 2012, 64(2): 271

7 Gao S, Hou J S, Yang F *et al. Materials Science and Engineering A*[J], 2017, 706: 153

8 Wu Y S, Zhang X X, Jiang L *et al. Materials Characterization*[J], 2025, 220: 114702

9 Geddes B, Leon H, Huang X. *Superalloys: Alloying and*

Performance[M]. Ohio: ASM International, 2010: 66
10 Reed R C. *The Superalloys: Fundamentals and Applications*[M]. Cambridge: Cambridge University Press, 2006
11 Chen J Y, Feng Q, Cao L M *et al. Materials Science and Engineering A*[J], 2011, 528(10–11): 3791
12 Chen Jingyang, Zhao Bing, Feng Qiang *et al. Acta Metallurgica Sinica*[J], 2010, 46(8): 897 (in Chinese)
13 Sims C T. *Superalloys: Genesis and Character*[M]. New York: John Wiley & Sons, 1987: 5
14 Collier J P, Keefe P W, Tien J K. *Metallurgical Transactions A*[J], 1986, 17(4): 651
15 Collins D M, Heenan R K, Stone H J. *Metallurgical and Materials Transactions A*[J], 2010, 42(1): 49
16 Han Xiaolei, Du Zhiwei, Che Cong *et al. Rare Metal Materials and Engineering*[J], 2023, 52(4): 1410 (in Chinese)
17 Qu Xinghui, Gao Lei, Wu Yidong *et al. Rare Metal Materials and Engineering*[J], 2025, 54(2): 490 (in Chinese)
18 Hou J S, Guo J T, Wu Y X *et al. Materials Science and Engineering A*[J], 2010, 527(6): 1548
19 Xu K D, Ren Z M, Li C J. *Rare Metals*[J], 2014, 33(2): 111
20 Wu Y X, Guo J, Hou J S *et al. Acta Metallurgica Sinica* (*English Letters*)[J], 2014, 27(1): 87
21 Zhang Y W, Wang F M, Hu B F. *Rare Metal Materials and Engineering*[J], 2012, 41(6): 989
22 Zhang Yiwen, Wang Fuming, Hu Benfu. *Acta Metallurgica Sinica*[J], 2012, 48(2): 187 (in Chinese)
23 Li L Z, Wu Y S, Hou J S *et al. Journal of Materials Research and Technology*[J], 2024, 30: 2977
24 Paraschiv A, Matache G, Puscasu C. *Transportation Research Procedia*[J], 2018, 29: 303
25 Gao S, Hou J S, Dong K X *et al. Acta Metallurgica Sinica* (*English Letters*)[J], 2016, 30(3): 261
26 Li X P, Xie Y S, Huang Y *et al. Rare Metal Materials and Engineering*[J], 2024, 53(10): 2952
27 Wang G, Song W, Liang J J *et al. Rare Metal Materials and Engineering*[J], 2024, 53(3): 787
28 Zhang Yiwen, Han Shoubo, Liu Jiantao *et al. The Chinese Journal of Nonferrous Metals*[J], 2016, 26(3): 535 (in Chinese)
29 Zhang H P, Bai J M, Li X K *et al. Journal of Materials Science*[J], 2022, 57(12): 6803
30 Lifshitz I M, Slyozov V V. *Journal of Physics and Chemistry of Solids*[J], 1961, 19(1–2): 35
31 Ardell A J, Nicholson R B. *Journal of Physics and Chemistry of Solids*[J], 1966, 27: 1793
32 Chen Jiayu, Zhang Panda, Dong Jianxin *et al. Chinese Journal of Engineering*[J], 2015, 37(12): 1610 (in Chinese)
33 Brandes E A, Brook G B. *Smithells Metals Reference Book*[M]. London: The Bath Press, 1992: 965
34 Hou Jieshan, Guo Jianting, Zhou Lanzhang *et al. Acta Metallurgica Sinica*[J], 2006, 42(5): 481 (in Chinese)
35 Pyczak F, Devrient B, Mughrabi H *et al. Proceedings of the International Symposium on Superalloys*[C], Warrendale: The Minerals, Metals & Materials Society, 2004: 827
36 Gornostyrev Y N, Kontsevoi O Y, Khromov K Y *et al. Scripta Materialia*[J], 2007, 56(2): 81
37 Reppich B, Schepp P, Wehner G. *Acta Metallurgica*[J], 1982, 30(1): 95
38 Shin K Y, Kim J H, Terner M *et al. Materials Science and Engineering A*[J], 2019, 751: 311
39 Chong Y, Liu Z D, Andy G *et al. Materials Science and Engineering A*[J], 2014, 589: 153
40 Oh J H, Choi I C, Kim Y J *et al*. *Materials Science and Engineering A*[J], 2011, 528(19–20): 6121
41 Reppich B. *Acta Metallurgica*[J], 1982, 30(1): 87
42 Orowan E. *Discussion on Internal Stresses in Metals and Alloys*[M]. London: The Institute of Metals, 1948, 451
43 Kozar R W, Suzuki A, Milligan W W *et al. Metallurgical and Materials Transactions A*[J], 2009, 40: 1588
44 Xu Y L, Yang C X, Xiao X S *et al. Materials Chemistry and Physics*[J], 2012, 134(2–3): 706
45 Ray P K, Akinc M, Kramer M J. *Journal of Alloys and Compounds*[J], 2010, 489(2): 357

铪合金化对Ni-Cr-Mo合金中γ′相沉淀行为及拉伸性能的影响

李林子[1,2]，管现军[1,3]，侯介山[1,3]，周兰章[1,3]
(1. 中国科学院 金属研究所 师昌绪先进材料创新中心，辽宁 沈阳 110016)
(2. 中国科学技术大学 材料科学与工程学院，辽宁 沈阳 110016)
(3. 中国科学院 金属研究所 核用材料与安全评价重点实验室，辽宁 沈阳 110016)

摘　要：研究了Hf对Ni-Cr-Mo合金长期热暴露后γ′相析出行为及拉伸性能的影响。结果表明，在700 ℃热暴露5000 h的过程中，Hf的加入增大了γ′相的尺寸，从而提高了Ni-Cr-Mo合金中位错剪切γ′相的临界分解剪切应力。同时，Hf元素进入γ′相中，增加了γ′与γ之间的晶格错配度，从而提高了沉淀强化效果。这2种因素共同提高了合金的强度。因此，Hf合金化可以有效地提高Ni-Cr-Mo合金在700 ℃高温下的屈服强度。

关键词：Ni-Cr-Mo合金；铪合金化；γ′强化；长时热暴露；位错剪切

作者简介：李林子，男，1994年生，博士，中国科学院金属研究所师昌绪先进材料创新中心，辽宁 沈阳 110016，电话：024-23971907，E-mail：lzli16s@imr.ac.cn